International Journal of Solids and Structures 49 (2012) 1656–1664

Contents lists available at SciVerse ScienceDirect

International Journal of Solids and Structures

journal homepage: www.elsevier.com/locate/ijsolstr

Buckling and post-buckling of a stiff film resting on an elastic graded substrate

Yan-Ping Cao *, Fei Jia, Yan Zhao, Xi-Qiao Feng *, Shou-Wen Yu

AML, Department of Engineering Mechanics, Tsinghua University, Beijing 100084, China

ARTICLE INFO

Article history:
Received 28 May 2011
Received in revised form 8 March 2012
Available online 20 March 2012

Keywords:
Surface wrinkling
Thin film
Elastic graded substrate
Analytical method
Finite element method

ABSTRACT

Systems consisting of a hard layer resting on an elastic graded soft substrate are frequently encountered both in nature and industry. In this paper, we study the surface wrinkling problem of such a composite system subjected to in-plane compression. The Young's modulus of the elastic substrate is assumed to vary along its depth direction. In particular, we investigate two typical variations in the modulus, described by a power function and an exponential function, respectively. Analytical solutions which permit to determine the critical compressive strain for the onset of wrinkling and the wrinkling wavelength are derived. A series of finite element simulations are performed to validate the theoretical solutions and demonstrate the prominent features of the postbuckling evolution of the system. The results may not only find applications in thin-film metrology and surface patterning but also provide insight into the wrinkling phenomena of various living tissues.

1. Introduction

Systems consisting of a hard layer resting on a soft substrate are often encountered in various natural and artificial materials and devices (Bowden et al., 1998; Ben Amar and Goriely, 2005; Li et al., 2011a). When subjected to in-plane compression, such a composite system may buckle and lose its original planar surface morphology. On one hand, surface instability represents a typical failure of materials or structures and should be avoided in most engineering designs (Allen, 1969), and, on the other hand, it also finds wide applications (Bowden et al., 1998; Ben Amar and Goriely, 2005; Li et al., 2011a; Bowden et al., 1999; Stafford et al., 2004; Efimenko et al., 2005; Lacour et al., 2005; Khang et al., 2006; Schweikart and Fery, 2009) and has received considerable interest from various disciplines in recent years. Micro-/nanosized surface patterns can endow solid materials with some unusual optical, electronic, and acoustic properties due to the effects of wave interference (Bowden et al., 1998, 1999). As well, surface patterns may significantly influence such properties as wetting, adhesion, and friction of solid surfaces (Koch et al., 2009; Chan et al., 2008; Feng et al., 2007; Wu-Bavouzet et al., 2010; Li et al., in press). Therefore, novel techniques have been proposed to create surfaces with controlled patterns on solid materials based on wrinkling phenomena of a thin stiff sheet resting on a compliant substrate.

Determining the mechanical properties of thin films is critical for their applications but still remains a challenging issue. Recently, enlightened by the buckling phenomenon of a thin film resting on a soft substrate (Bowden et al., 1998), Stafford et al. (2004) presented a novel method to measure the elastic modulus of a thin film. They showed that this methodology can be applied to the mechanical characterization of thin films, even when the film thickness reduces to nanometers.

In nature, many living soft tissues including skins, brains, ciliary body and mucosa of esophagus and pulmonary airway can also be modeled as a soft substrate covered by a thin and hard surface layer (Li et al., 2011a). It is noted that the sub-surface layer (substrate) usually has gradient mechanical properties because of the spatial variation in the microstructure and/or composition. Surface wrinkling/folding observed in these living tissues is, on one hand, believed to play a significant physiological role in healthy biological tissues. On the other hand, such diseases as inflammation, edema, asthma and enterogastritis may induce the variation of the surface morphology of soft tissues (Li et al., 2011a). Therefore, the alteration of wrinkling patterns may be regarded as an important clinical sign and symptom of some diseases.

Given the technical and scientific importance, much effort has been devoted toward revealing the underlying physical mechanisms behind the occurrence of surface instabilities of a hard layer lying on a soft substrate (Groenewold, 2001; Cerda and Mahadevan, 2003; Huang, 2005; Huang et al., 2005; Audoly and Boudaoud, 2008a,b,c; Cai et al., 2011). Most previous studies assume a homogeneous substrate. However, many practical systems have an elastic graded substrate (Howarter and Stafford, 2010). For example, the deposition of a hard film on a soft substrate may lead to the variation in the mechanical property of the substrate along the depth direction, especially in the vicinity of the substrate

* Corresponding authors. Tel.: +86 10 6277 2934; fax: +86 10 6278 1824.
E-mail addresses: caoyanping@tsinghua.edu.cn (Y.-P. Cao), fengxq@tsinghua.edu.cn (X.-Q. Feng).

0020-7683/$ - see front matter © 2012 Elsevier Ltd. All rights reserved.
http://dx.doi.org/10.1016/j.ijsolstr.2012.03.004

surface (Howarter and Stafford, 2010). To date, nevertheless, there is a shortage of theoretical investigation on the instability of a hard layer resting on an elastic graded substrate. Recently, Lee et al. (2008) performed a bifurcation analysis for the surface wrinkling of an elastic half-space under in-plane compression, in which the Young's modulus varies arbitrarily along the depth. They developed a finite element method (Lee et al., 2008) to solve this problem.

In the present paper, theoretical analysis is carried out for a hard film wrinkling on an elastic graded substrate subjected to in-plane compression. In particular, we explore two typical variations in the substrate modulus along the depth direction, which can be expressed by a power function and an exponential function, respectively. Closed-form expressions of the compressive force acting on the hard layer are given, which allow a straightforward determination of the critical compressive strain for the onset of the surface buckling and the wrinkling wavelength. Finite element simulations are performed to validate our theoretical solutions and to examine the postbuckling behavior of the composite system.

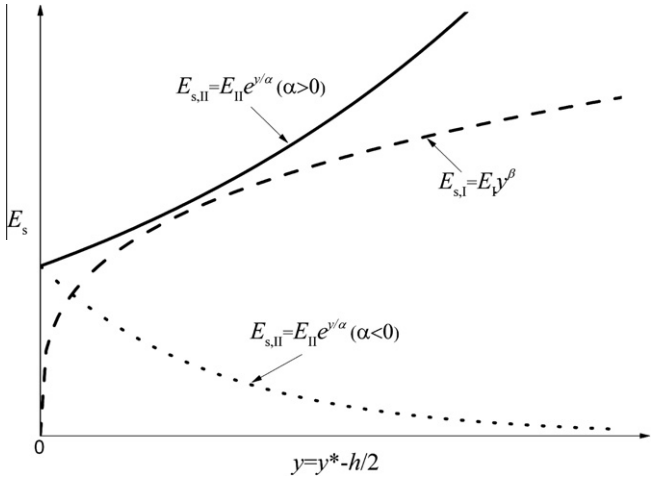

Fig. 2. Variations of the Young's modulus of the substrate along the depth.

2. Theoretical analysis

2.1. Models

Consider a composite system consisting of a stiff layer resting on a soft and semi-infinite substrate, subjected to uniaxial in-plane compression. Refer to a Cartesian coordinate system (O–xy^*), as shown in Fig. 1, where the origin O is located at the center of the film, the x and y^* axes are along and normal to the surface layer, respectively. Assume that the film is linear elastic, isotropic, and homogeneous. The substrate has a constant Poisson's ratio but its Young's modulus varies along the depth direction. We here consider the following two representative variations in the modulus (Fig. 2), which have been widely used to explore the response of an elastic graded solid (Gibson, 1967; Plevako, 1971; Giannakopoulos and Suresh, 1997; Giannakopoulos and Pallot, 2000; Muravskii, 2008; Chen et al., 2009).

Case I: Power-law grading modulus

$$E_{s,\,I} = E_I y^{\beta} \tag{1}$$

where E_I and β are material constants. Here and in Fig. 2, the coordinate $y = y^* - h/2$ with h being the film thickness. β varies from 0 to 1. $\beta = 1$ corresponds to the so-called Gibson soil (Gibson, 1967). It is noted that E_I is not necessary to have the dimension of elastic modulus. In this model, the solid has zero modulus at the surface, which may not be realistic. But this simple model permits to obtain closed-form solutions in many cases.

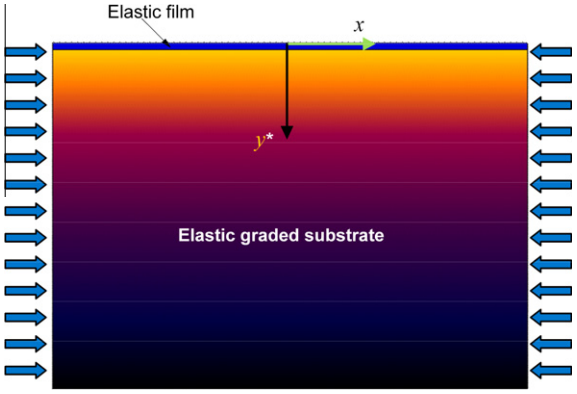

Fig. 1. A stiff layer resting on an elastic graded substrate under in-plane compression.

Case II: Exponential grading modulus

$$E_{s,\,II} = E_{II} \exp\left(\frac{y}{\alpha}\right) \tag{2}$$

where E_{II} and α are material constants. Here α can be positive or negative as shown in Fig. 2.

In the sequel, we will analyze the wrinkling of an elastic film resting on a power-law graded substrate (Case I) and an exponential graded substrate (Case II), respectively.

2.2. Wrinkling of a stiff film resting on a power-law graded soft substrate

Linear perturbation analysis is performed to predict the critical compressive strain at the onset of wrinkling and the corresponding wrinkling wavelength by modeling the film as a plate. In many previous theoretical analyses on the wrinkling of a film resting on a soft substrate (Volynskii et al., 2000; Huang et al., 2005; Jia et al., in press), shear stresses between the film and the substrate are assumed to be zero. This may lead to significant errors when Poisson's ratio of the substrate is small. In this analysis, the effects of interfacial shear stresses are accounted for following a recent study of Mei et al. (2011), who considered a homogeneous substrate. When the deflection w and in-plane displacement u in the film are small, the equilibrium condition of the film reads (Mei et al., 2011)

$$\begin{aligned} \sigma_n &= -\frac{E_f^* h^3}{12}\frac{d^4 w}{dx^4} + \varepsilon E_f^* h \frac{d^2 w}{dx^2}, \\ \tau_s &= E_f^* h \frac{d^2 u}{dx^2}, \end{aligned} \tag{3}$$

where $E_f^* = E_f/(1-\nu_f^2)$ is the plane-strain elastic modulus of the film, E_f and ν_f are the elastic modulus and Poisson's ratio of the film, respectively. σ_n and τ_s are the normal and shear stress at the film/substrate interface. Here ε is the nominal compressive strain. Assume that the film is perfectly bonded to the substrate. In this case, a key issue in the wrinkling analysis is to determine the surface displacements of the substrate subjected to the following surface tractions

$$\begin{aligned} \sigma_n &= \sigma_{n,0}\cos(\omega x) \\ \tau_s &= \tau_{s,0}\sin(\omega x) \end{aligned} \tag{4}$$

where ω is the wavenumber. Recently, Muravskii (2008) derived the solution for the surface displacements of a power-law graded half-space under a vertical line load F as

$$w_1(x,y=0)=\frac{(1-\nu_s^2)qCF}{E_1(1+\beta)\beta}|x|^{-\beta}\sin\frac{\pi q}{2}=B_1F|x|^{-\beta} \tag{5a}$$

$$u_1(x,y=0)=\frac{(1-\nu_s^2)CF}{E_1\beta}\frac{x}{|x|^{1+\beta}}\cos\frac{\pi q}{2}=B_2F\frac{x}{|x|^{1+\beta}} \tag{5b}$$

and those under a horizontal line load T as

$$w_2(x,y=0)=-\frac{(1-\nu_s^2)CT}{E_1\beta}\frac{x}{|x|^{1+\beta}}\cos\frac{\pi q}{2}=D_1T\frac{x}{|x|^{1+\beta}} \tag{6a}$$

$$u_2(x,y=0)=\frac{(1-\nu_s^2)(1+\beta)CT}{E_1q\beta}|x|^{-\beta}\sin\frac{\pi q}{2}=D_2T|x|^{-\beta} \tag{6b}$$

with

$$C=\frac{2^{1+\beta}}{\pi\Gamma(2+\beta)}\Gamma\left(\frac{3+\beta+q}{2}\right)\Gamma\left(\frac{3+\beta-q}{2}\right), \tag{7}$$

where Γ is the Gamma function,

$$q=\sqrt{(1+\beta)[1-\beta\nu_s/(1-\nu_s)]} \tag{8}$$

$$B_1=\frac{b_1}{E_1^*},\quad B_2=\frac{b_2}{E_1^*},\quad D_1=-\frac{d_1}{E_1^*},\quad D_2=\frac{d_2}{E_1^*} \tag{9}$$

$E_1^*=E_1/(1-\nu_s^2)$, ν_s is the Poisson's ratio of the substrate, and

$$b_1=\frac{qC}{(1+\beta)\beta}\sin\frac{\pi q}{2},\quad b_2=d_1=\frac{C}{\beta}\cos\left(\frac{\pi q}{2}\right),\quad d_2=\frac{(1+\beta)C}{q\beta}\sin\left(\frac{\pi q}{2}\right). \tag{10}$$

In this paper, we invoke Muravskii's solution given above to solve the surface displacements of the substrate under the surface tractions in Eq. (4). Using Eqs. (5) and (6) and the superposition principle, we obtain

$$\begin{aligned} w&=2\left(\sigma_{n,0}B_1\int_0^{+\infty}\frac{\cos\omega t}{t^\beta}dt+\tau_{s,0}D_1\int_0^{+\infty}\frac{\sin\omega t}{t^\beta}dt\right)\cos\omega x\\ u&=2\left(-\sigma_{n,0}B_2\int_0^{+\infty}\frac{\sin\omega t}{t^\beta}dt+\tau_{s,0}D_2\int_0^{+\infty}\frac{\cos\omega t}{t^\beta}dt\right)\sin\omega x \end{aligned} \tag{11}$$

where

$$\int_0^{+\infty}\frac{\sin\omega t}{t^\beta}dt=\omega^{\beta-1}\cos\frac{\pi\beta}{2}\Gamma(1-\beta), \tag{12a}$$

$$\int_0^{+\infty}\frac{\cos\omega t}{t^\beta}dt=\omega^{\beta-1}\sin\frac{\pi\beta}{2}\Gamma(1-\beta). \tag{12b}$$

Letting

$$c_1=\cos\left(\frac{\pi\beta}{2}\right)\Gamma(1-\beta),\quad c_2=\sin\left(\frac{\pi\beta}{2}\right)\Gamma(1-\beta), \tag{13}$$

and inserting Eq. (11) into (3), we have

$$\left[b_1c_2+\frac{E_1^*\omega^{1-\beta}}{2E_f^*\omega}\left(\frac{1}{12}(h\omega)^3+\varepsilon h\omega\right)^{-1}\right]\sigma_{n,0}+d_1c_1\tau_{s,0}=0, \tag{14a}$$

$$-b_2c_1\sigma_{n,0}+\left[d_2c_2+\frac{E_1^*\omega^{1-\beta}}{2E_f^*\omega}\frac{1}{h\omega}\right]\tau_{s,0}=0. \tag{14b}$$

By setting the determinant of the coefficient matrix in Eq. (14) to zero, the critical strain can be obtained as

$$\varepsilon_c=\frac{(h\omega)^2}{12}+\frac{E_1^*\omega^{1-\beta}}{E_f^*\omega}\times\frac{1}{2h\omega}\left[b_1c_2-b_2d_1c_1^2\left(d_2c_2+\frac{E_1^*\omega^{1-\beta}}{E_f^*\omega}\frac{1}{2h\omega}\right)^{-1}\right]^{-1}. \tag{15}$$

For a stiff film resting on a soft substrate, $\frac{E_1^*\omega^{1-\beta}}{2E_f^*\omega^2h}\ll d_2c_2$, Eq. (15) reduces to

$$\varepsilon_c=\frac{(h\omega)^2}{12}+\frac{E_1^*\omega^{-1-\beta}}{E_f^*}\frac{1}{2h}\left[b_1c_2-b_2d_1c_1^2(d_2c_2)^{-1}\right]^{-1}. \tag{16}$$

Eq. (16) can be rewritten as

$$\varepsilon_c=\frac{(h\omega)^2}{12}+\frac{E_1^*\omega^{-1-\beta}}{E_f^*}\frac{\Pi_1}{h}\left[1-\frac{1}{\tan^2(\pi q/2)\tan^2(\pi\beta/2)}\right]^{-1}, \tag{17}$$

where

$$\Pi_1=\frac{(1+\beta)\beta}{2qC\Gamma(1-\beta)\sin\frac{\pi\beta}{2}\sin\frac{\pi q}{2}}. \tag{18}$$

When $\beta\to0$, the critical strain in Eq. (17) reduces to the following solution for the homogeneous substrate case, which was derived by Mei et al. (2011),

$$\varepsilon_{c,h}=\frac{(h\omega)^2}{12}+\frac{E_1^*}{2hE_f^*\omega}\left[1-\frac{1}{4}\left(\frac{1-2\nu_s}{1-\nu_s}\right)^2\right]^{-1}. \tag{19}$$

Denote

$$\xi=1-\frac{1}{\tan^2(\pi q/2)\tan^2(\pi\beta/2)}. \tag{20}$$

Then the minimization of ε_c in Eq. (17) with respect to ω gives the critical wrinkling wavelength as the following closed-form

$$\lambda_{1,c}=2\pi h\left[\frac{E_f^*h^{-\beta}\xi}{6(1+\beta)E_1^*\Pi_1}\right]^{\frac{1}{3+\beta}}. \tag{21}$$

Correspondingly the minimum critical strain $\varepsilon_{c,I}$ is

$$\varepsilon_{c,I}=\frac{(h\omega_c)^2}{12}+\frac{E_1^*\omega_c^{-1-\beta}}{E_f^*}\frac{\Pi_1}{h}\left[1-\frac{1}{\tan^2(\pi q/2)\tan^2(\pi\beta/2)}\right]^{-1}, \tag{22}$$

where $\omega_c=2\pi/\lambda_{1,c}$. When $\beta\to0$, the critical wrinkling wavelength $\lambda_{1,c}$ and the minimum critical strain $\varepsilon_{c,I}$ reduce to the solutions of Mei et al. (2011) for a homogeneous substrate.

2.3. Wrinkling of a stiff film on an exponential graded soft substrate

For the substrate with grading modulus given by the exponential function (Eq. (2)), we first derive the surface displacements under the surface tractions given by Eq. (4). Here we adopted the following equilibrium equation proposed by Plevako (1971) for a plane strain problem

$$\Delta\left(\frac{1}{G}\Delta L\right)-\frac{1}{1-\nu_s}\frac{\partial^2L}{\partial x^2}\frac{d^2}{dy^2}\left(\frac{1}{G}\right)=0, \tag{23}$$

where $\Delta=\partial^2/\partial x^2+\partial^2/\partial y^2$ represents the Laplace operator. The shear modulus G is related to the elastic modulus of the substrate by

$$G=\frac{E_{s,II}}{2(1+\nu_s)}=\frac{E_{II}}{2(1+\nu_s)}e^{\frac{y}{\xi}}. \tag{24}$$

In Eq. (23), L is a function defined by Plevako (1971). It gives the stresses and displacements in the substrate as

$$\sigma_x = \frac{\partial^4 L}{\partial x^2 \partial y^2}, \quad \sigma_y = \frac{\partial^4 L}{\partial x^4}, \tag{25a}$$

$$\tau_{xy} = -\frac{\partial^4 L}{\partial x^3 \partial y}, \tag{25b}$$

$$u_s = -\frac{1}{2G}\left[\nu_s \frac{\partial^2}{\partial x^2} - (1-\nu_s)\frac{\partial^2}{\partial y^2}\right]\frac{\partial L}{\partial x}, \tag{25c}$$

$$w_s = -\frac{1}{G}\frac{\partial^3 L}{\partial^2 x \partial y} + \frac{\partial}{\partial y}\left[\frac{1}{2G}\left(\nu_s \frac{\partial^2 L}{\partial x^2} - (1-\nu_s)\frac{\partial^2 L}{\partial y^2}\right)\right], \tag{25d}$$

where u_s and w_s represent the displacements in the x and y directions, respectively. We apply the method of separation of variables and assume

$$L = \phi(y)\cos(\omega x). \tag{26}$$

Substituting (26) into (23) leads to the following fourth-order differential equation

$$\phi^{(4)} - \frac{2}{\alpha}\phi^{(3)} + \left(\frac{1}{\alpha^2} - 2\omega^2\right)\phi'' + \frac{2\omega^2}{\alpha}\phi' + \left(\omega^4 + \frac{\omega^2}{\alpha^2}\frac{\nu_s}{1-\nu_s}\right)\phi = 0. \tag{27}$$

Its characteristic equation is

$$\left(\frac{\kappa}{\omega}\right)^4 - \frac{2}{\alpha\omega}\left(\frac{\kappa}{\omega}\right)^3 + \left(\frac{1}{\alpha^2\omega^2} - 2\right)\left(\frac{\kappa}{\omega}\right)^2 + \frac{2}{\alpha\omega}\frac{\kappa}{\omega} + \left(1 + \frac{1}{\alpha^2\omega^2}\frac{\nu_s}{1-\nu_s}\right) = 0. \tag{28}$$

Set

$$\frac{\kappa}{\omega} = \gamma + \frac{1}{2\alpha\omega}, \tag{29}$$

then, Eq. (28) is rewritten as

$$\gamma^4 - \frac{1+4\alpha^2\omega^2}{2\alpha^2\omega^2}\gamma^2 + \left(\frac{1}{16\alpha^4\omega^4} + \frac{1}{2\alpha^2\omega^2}\frac{1+\nu_s}{1-\nu_s} + 1\right) = 0. \tag{30}$$

From Eqs. (29) and (30), we get the following two characteristic roots

$$\frac{\kappa}{\omega} = \pm\sqrt{\frac{1+4\alpha^2\omega^2}{4\alpha^2\omega^2} \pm \sqrt{\frac{1}{\alpha^2\omega^2}\frac{\nu_s}{1-\nu_s}}\mathrm{i}} + \frac{1}{2\alpha\omega}, \tag{31}$$

where i is the imaginary unit.

By setting

$$\frac{1+4\alpha^2\omega^2}{4\alpha^2\omega^2} \pm \sqrt{\frac{1}{\alpha^2\omega^2}\frac{\nu_s}{1-\nu_s}}\mathrm{i} = re^{\mp \mathrm{i}\theta}, \tag{32}$$

then Eq. (31) becomes

$$\frac{\kappa}{\omega} = \pm A' + \frac{1}{2\alpha\omega} \pm \mathrm{i}B, \tag{33}$$

where

$$A' = \sqrt{r}\cos\left(\frac{1}{2}\theta\right) \quad B = \sqrt{r}\sin\left(\frac{1}{2}\theta\right). \tag{34}$$

Further, we let $A = -A' + \frac{1}{2\alpha\omega}$, then the solution of L is obtained as:

$$L = \begin{pmatrix} (e^{A\omega y}(C_1\sin(B\omega y) + C_2\cos(B\omega y)) \\ +e^{(A'+\frac{1}{2\alpha\omega})\omega y}(C_3\sin(B\omega y) + C_4\cos(B\omega y)) \end{pmatrix}\cos(\omega x), \tag{35}$$

where the constants C_1–C_4 are yet to be determined from the boundary conditions:

$$-\sigma_y(y=0) = \sigma_{n,0}\cos(\omega x), -\tau_{xy}(y=0) = \tau_{s,0}\sin(\omega x) \tag{36a}$$

$$\sigma_y(y=\infty) = 0, \quad \tau_{xy}(y=\infty) = 0. \tag{36b}$$

Eq. (36b) requires that $C_4 = C_3 = 0$. The stresses based on (25a) and (25b) can be expressed as

$$\sigma_y = \frac{\partial^4 L}{\partial x^4} = e^{A\omega y}(C_1\sin(B\omega y) + C_2\cos(B\omega y))\omega^4\cos(\omega x), \tag{37a}$$

$$\tau_{xy} = -\frac{\partial^4 L}{\partial x^3 \partial y} = -e^{Awy}[(AC_1 - BC_2)\sin(B\omega y) + (AC_2 + BC_1)\cos(B\omega y)]\omega^4\sin(\omega x). \tag{37b}$$

Eqs. (37) and (36a) give

$$C_2 = -\frac{\sigma_{n,0}}{\omega^4} \quad C_1 = \frac{1}{B\omega^4}(\tau_{n,0} + A\sigma_{n,0}). \tag{38}$$

Using Eq. (25), the surface displacements are determined

$$w = (g_1\sigma_{n,0} + g_2\tau_{n,0})\frac{1}{E_{II}^*\omega}\cos(\omega x), \tag{39a}$$

$$u = (g_3\sigma_{n,0} + g_4\tau_{n,0})\frac{1}{E_{II}^*\omega}\sin(\omega x), \tag{39b}$$

where $E_{II}^* = E_{II}/(1-\nu_s^2)$, and

$$g_1 = -\left[\frac{\nu_s}{1-\nu_s}\frac{1}{\alpha\omega} + (A^2+B^2)\left(-\frac{1}{\alpha\omega} + 2A\right)\right], \quad g_2 = \left[1 + \frac{1}{1-\nu_s} + \frac{2A}{\alpha\omega} - (3A^2 - B^2)\right], \tag{40}$$

$$g_3 = \left[\frac{\nu_s}{1-\nu_s} - (A^2+B^2)\right], \quad g_4 = -2A. \tag{41}$$

Inserting Eqs. (39) and (4) into Eq. (3) leads to

$$\left[g_1 + \frac{E_{II}^*}{E_f^*}\left(\frac{1}{12}(h\omega)^3 + \varepsilon h\omega\right)^{-1}\right]\sigma_{n,0} + g_2\tau_{n,0} = 0, \tag{42}$$

$$g_3\sigma_{n,0} + \left(g_4 + \frac{E_{II}^*}{E_f^*}\frac{1}{h\omega}\right)\tau_{n,0} = 0. \tag{43}$$

By setting the determinant of the coefficient matrix in Eq. (43) to zero, the critical strain is obtained as

$$\varepsilon_c = \frac{(h\omega)^2}{12} + \frac{E_{II}^*}{E_f^*}\frac{1}{h\omega}\left[g_1 - g_2g_3\left(g_4 + \frac{E_{II}^*}{E_f^*}\frac{1}{h\omega}\right)^{-1}\right]^{-1}. \tag{44}$$

For a stiff film resting on a soft substrate, $\frac{E_{II}^*}{E_f^*h\omega} \ll g_4$, Eq. (44) reduces to

$$\varepsilon_c = \frac{(h\omega)^2}{12} + \frac{E_{II}^*}{E_f^*}\frac{1}{g_1h\omega}\left[1 - \frac{g_2g_3}{g_1g_4}\right]^{-1}. \tag{45}$$

When $|\alpha\omega| \to \infty$, Eq. (45) degenerates to Eq. (11) in Mei et al. (2011) for a homogeneous substrate.

For given physical and geometric parameters of the system, the critical wrinkling wavelength $\lambda_{II,c}$ can be obtained by searching ω which minimizes the critical strain in (44) or (45). ε_c corresponding to $\omega = 2\pi/\lambda_{II,c}$ is the minimum critical compressive strain $\varepsilon_{c,II}$ for the onset of wrinkling.

3. Numerical validation

In the above theoretical analysis, the film is modeled as a plate. This requires that the wrinkling wavelength is much greater than the film thickness and hence the film modulus should be much greater than that of the substrate. In this section, finite element simulations are carried out to demonstrate that the theoretical solutions can predict both the critical compressive strain and wrinkling wavelength correctly, and to identify the ranges of material parameters in which the theoretical solutions are applicable.

Eight-node plane-strain quadrilateral reduced integration elements (CPE8R) are used to mesh the system. Convergence of the computational results is carefully examined. Very fine meshes are adopted to discretize the film and the region of the substrate near the interface. The maximum ratio of the wrinkling wavelength to the element size is as large as 5000 in order to ensure the high accuracy of the simulation results.

The linear perturbation analysis is accomplished by using the BUCKLE function in ABAQUS to determine the critical compressive strain and the wrinkling wavelength. For a typical case, Figs. 3 and 4 compare the theoretical and numerical results for the critical compressive strain and the wrinkling wavelength. For all examples the finite element results match very well with the theoretical solution. To identify the material parameter range in which the theoretical solutions can predict wrinkling feature with a high level of accuracy, a series of simulations have been performed. We explore the parameter range with $0 \leqslant \beta \leqslant 1$, $\alpha/h \leqslant -40$ and $\alpha/h > 5$, $E_f/(E_1 l^\beta) \geqslant 5$ and $E_f/E_{II} \geqslant 5$. Here l represents the unit length. Our results indicate for both the power-law graded substrate and the exponential graded substrate, when the ratios of $E_f/(E_1 l^\beta)$ and E_f/E_{II} are larger than 20, the present theoretical solutions match the finite element results very well. It should be pointed out that this study focuses on the surface wrinkling behavior; but for $\alpha < 0$ and when the substrate is long enough, a buckling mode similar to the Euler buckling may occur first, which is beyond the scope of this work.

4. Postbuckling evolution

The above theoretical analysis focuses on the critical buckling of the system. In this section, we perform nonlinear finite element simulations to examine the postbuckling evolution of the system using a pseudo dynamic solution method, which has been successfully applied in recent studies (Li et al., 2011a,b; Mueller et al., 2008). In the post-buckling analysis, the incompressible neo-Hookean constitutive model is applied to characterize the deformation of film and the substrate, with the strain energy function given by

$$W = \frac{\mu}{2}(\alpha_1^2 + \alpha_2^2 + \alpha_3^2 - 3), \tag{46}$$

where α_i ($i = 1, 2, 3$) stand for the principal stretches along the x_i direction and μ is the initial shear modulus. Eight-noded plane-strain hybrid elements (CPE8RH) are used for both the film and the substrate. A linear perturbation procedure is accomplished using the "buckle" function in the software. The critical eigenmode scaled by a small factor is introduced as a geometric imperfection into the mesh. The ratio between the amplitude of the initial imperfection to the film thickness is taken as $A_0/h = 0.05$, which triggers smoothly the wrinkling. In the post-buckling analysis, displacement-controlled loading is employed with the displacement in x direction and zero shear traction specified on the vertical sides of the model. The nominal compressive overall strain ε_T applied to the system in the post-buckling process is defined as the total compressive amount divided by the original length of the model with the geometric imperfection introduced. On the bottom surface, the displacement in y direction and the shear traction are taken to be zero.

We first simulate the postbuckling evolution of a planar film resting on a soft homogeneous substrate subjected to in-plane compression. The ratio between the shear moduli of the film and the substrate is taken as 500. When the compression strain reaches a critical value, regular sinusoidal wrinkles may emerge (Fig. 5a). Further compression will trigger a period-doubling buckling morphology (Fig. 5b). The critical compressive strain at which the buckling morphology transition occurs is around 20%. The results agree well with the recent experiment of Brau et al. (2011), in which a thin stiff PDMS film bonded to a thick soft PDMS foundation is subjected to in-plane compression, as shown in Fig. 5c and d.

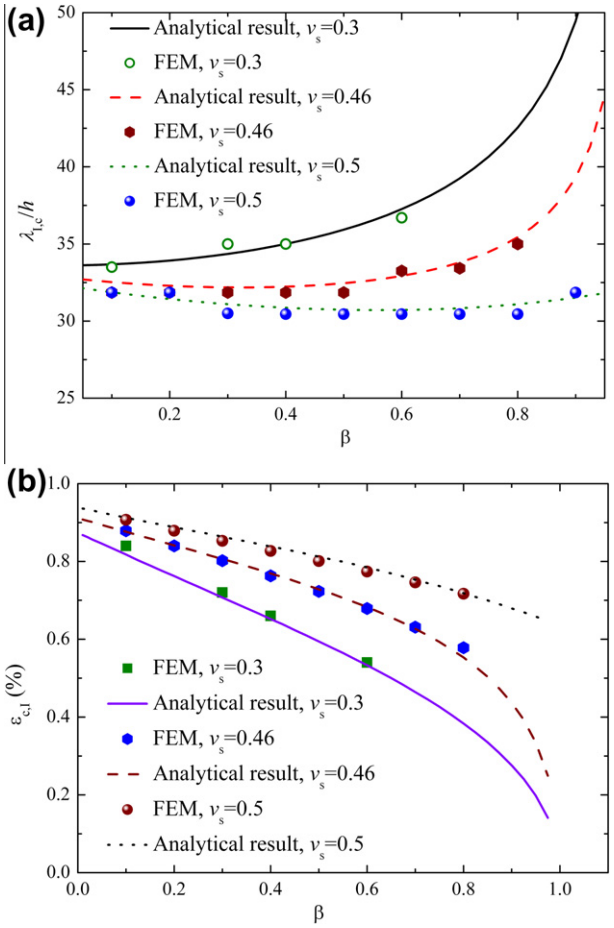

Fig. 3. Comparison between the theoretical and finite element results, where we take E_f = 10 GPa, ν_f = 0.3, h_f = 0.1 mm, and E_1 = 20 MPa · mm$^{1-\beta}$. (a) Critical wrinkling wavelength, and (b) critical compressive strain.

We further simulate the postbuckling evolution of a stiff film resting on a soft elastic graded substrate. Three representative cases are investigated, in which the shear modulus of the incompressible hyperelastic substrate varies with respect to the depth, y, via the functions (i) $\mu_s = 20y^{0.5}$ MPa, (ii) $\mu_s = 20\exp(-y/8)$ MPa, and (iii) $\mu_s = 20\exp(y/8)$ MPa, respectively. For all the examples, the film's shear modulus is taken as 10 GPa. Several snapshots are given in Fig. 6(a–f). It is shown that for all cases, the film first buckles into a wavy sinusoidal morphology. Here we examine how the wrinkling wavelength evolves from the occurrence of the sinusoidal wrinkling to the period-doubling wrinkling stage with the increase in the compressive strain. We monitor a wave in the center region, and Fig. 7 shows the variation in the wrinkling wavelength with the increase of the compressive strain ε_T for exponential graded substrates. Brau et al. (2011) have proposed a simple formula for homogeneous substrates to predict the variation in the wrinkling wavelength by assuming that the film is inextensible during the post-buckling stage. Our analysis finds that for elastic graded substrates the prediction given by this simple relation (solid line in Fig. 7) matches the finite element results (points in Fig. 7) remarkably well till the occurrence of period-doubling mode. In addition, our post-buckling simulations clearly demonstrate that the modulus gradient of the substrate has a marked effect on the postbuckling morphological evolution. In both cases (i) and (ii),

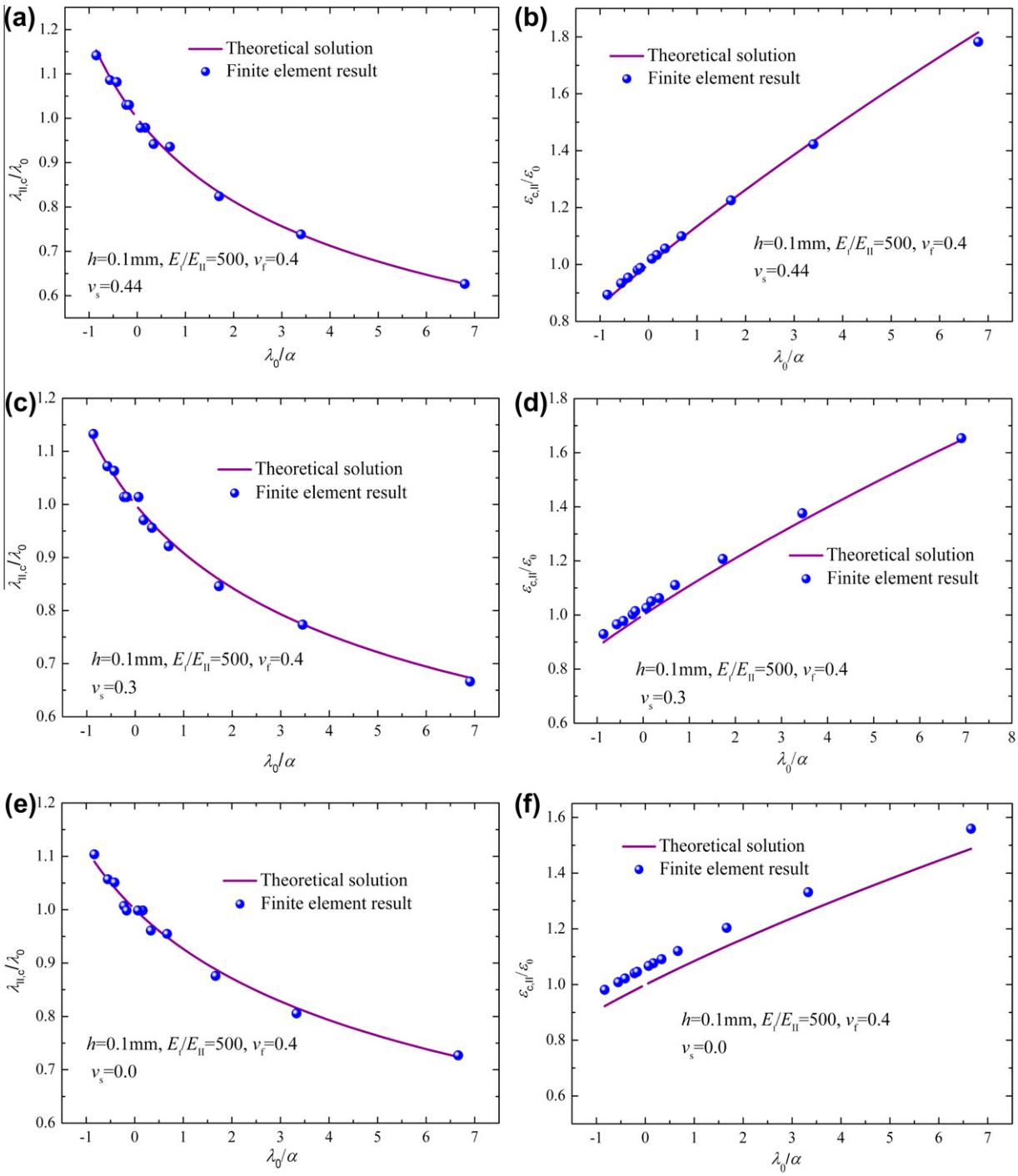

Fig. 4. Comparison of our theoretical results with finite element results. The variation in the elastic modulus is described by Eq. (2). (a) Critical wrinkling wavelength under $\upsilon_s = 0.44$, (b) critical compressive strain of buckling under $\upsilon_s = 0.44$, (c) critical wrinkling wavelength under $\upsilon_s = 0.3$, (d) critical compressive strain of buckling under $\upsilon_s = 0.3$, (e) critical wrinkling wavelength under $\upsilon_s = 0$, and (f) critical compressive strain of buckling under $\upsilon_s = 0$. ε_0 and λ_0 are the critical compressive strain and the wrinkling wavelength for a homogeneous substrate ($|\alpha| \to \infty$), which are calculated using the theoretical solutions of Mei et al. (2011).

the shear modulus of the substrate increases from its surface to interior. For case (i), no surface pattern transformation is observed when the compressive strain is up to 30%. In case (ii), surface pattern transformation occurs but the critical compressive strains are greater than those corresponding to the homogeneous substrate. When the shear modulus decreases from the boundary to the interior (case (iii), the surface pattern may evolve into doubling-period or multi-periodic topography at a smaller compressive strain. Notwithstanding these interesting results are insightful and may be useful in practice, the underlying physical mechanisms are not well understood and deserve further theoretical and experimental efforts.

5. Discussion

The above analysis has revealed some prominent features for the wrinkling behavior of a hard layer resting on an elastic graded soft substrate. First, the theoretical results permit to examine how the variation of the Young's modulus in the substrate influences

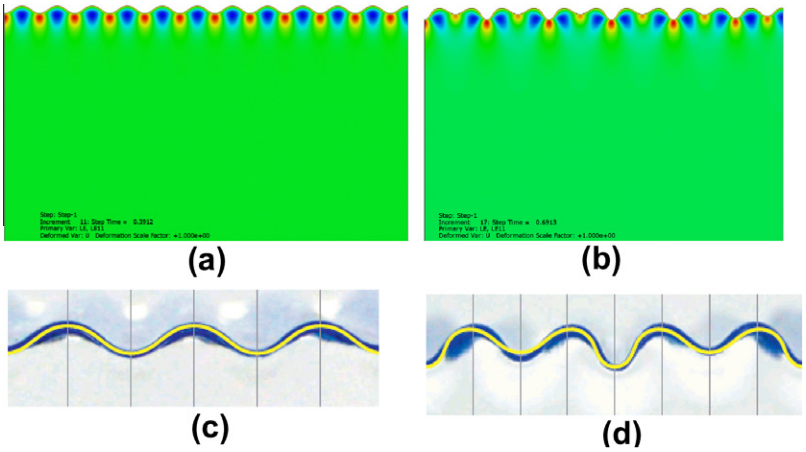

Fig. 5. Compression-induced postbuckling evolution of the planar film-homogeneous substrate system: (a) and (b) are finite element results for the compressive strain $\varepsilon_A = 11.7\%$ and $\varepsilon_A = 20.7\%$, respectively; (c) and (d) represent experimental results (Brau et al., 2011) for $\varepsilon_A = 11\%$ and $\varepsilon_A = 19\%$, respectively.

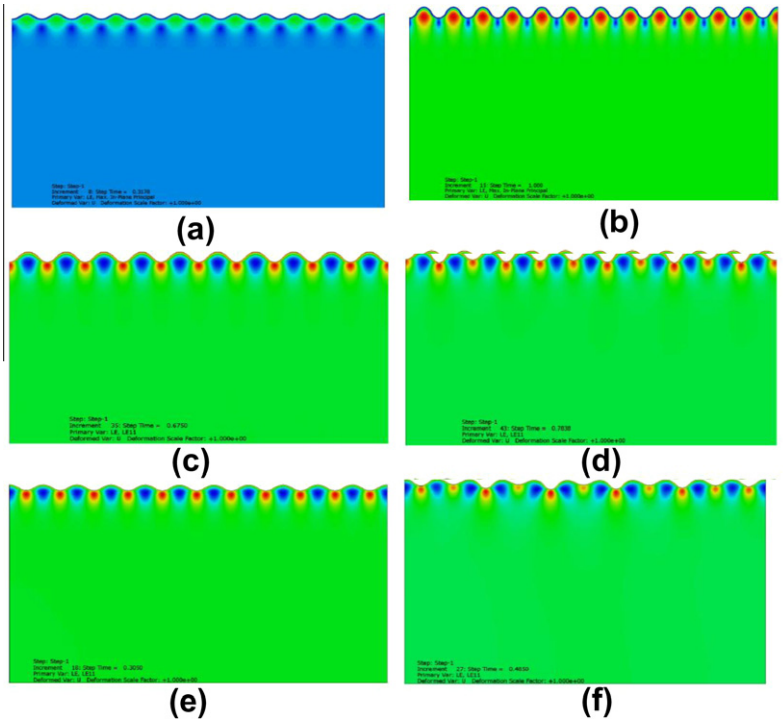

Fig. 6. Evolution of postbuckling for the film resting on an elastic graded substrate under in-plane compression. (a) and (b) are the buckling morphology for case (i) at the compressive strain of $\varepsilon_A = 9.6\%$ and $\varepsilon_A = 30\%$, respectively; (c) and (d) represent the buckling morphology for case (ii) at the compressive strain of $\varepsilon_A = 20\%$ and $\varepsilon_A = 23.5\%$, respectively; (e) and (f) are the surface pattern for case (iii) at the compressive strain of $\varepsilon_A = 9\%$ and $\varepsilon_A = 14.5\%$, respectively.

the onset of the buckling and the surface wrinkling wavelength. Taking the case where the modulus varies in a power function as an example, Fig. 3 illustrates that for a substrate with a high Poisson ratio, the value of β does not have a significant influence on the wrinkling wavelength. Thus, the substrate may be simplified as a homogeneous one for the critical buckling analysis provided that the substrate is nearly incompressible. For a hard film resting on a homogeneous substrate, Brau et al. (2011) showed that there exists a critical compressive strain beyond which the sinusoidal buckling mode may evolve into the doubling-period buckling morphology. Such a critical strain depends only on the Poisson's ratio of the substrate and is basically independent of the ratio of the film modulus to that of the substrate (Brau et al., 2011). For a stiff film resting on an elastic graded substrate, our post-buckling analysis shows the gradient of the elastic modulus of the substrate has significant effects on the buckling morphological evolution under a given Poisson's ratio. Besides the potential applications as discussed in the introduction part, the results may also help improve anti-wrinkling techniques. Recently, Hendricks and Lee (2007) reported that for a PEM film resting on a PDMS substrate, the incorporation of silica nanoparticles into the film may alleviate the compressive stress and prevent buckling. The present theoretical results indicate another possibility to prevent wrinkling. When nanoparticles are incorporated into the film/substrate system, they may diffusion into the surface layer of the substrate, rendering a gradient variation of the Young's modulus along the depth direction. As a consequence, the critical compressive strain can be significantly increased in comparison with that without surface treatment according to the present theoretical analysis and hence wrinkling may be prevented.

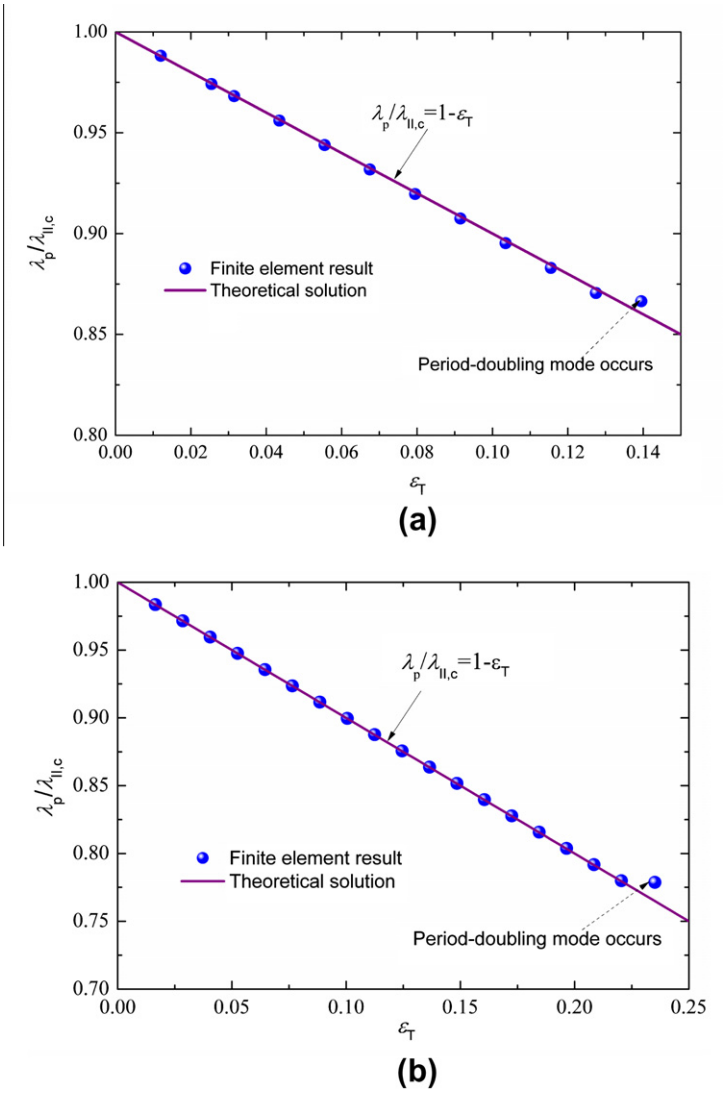

Fig. 7. Evolution of the postbuckling wavelength λ_p from the occurrence of the sinusoidal wrinkling to the beginning of period-doubling as the compressive strain increases. (a) $\alpha/h = -80$; (b) $\alpha/h = 80$. Points: finite element results; solid lines: theoretical prediction. $\lambda_{II,c}$ in the figure is given by the "BUCKLE" analysis, which perfectly matches that calculated using Eq. (45) by replacing E^*_{II} and E^*_f with the initial shear modulus at the surface of the substrate $\mu_s(0)$ and that of the film μ_f.

Finally, the limitations in this study are emphasized as follows. Firstly, there often exists a certain magnitude of residual stresses/strains in practical systems, which may affect the critical compressive strain though their influence on the wrinkling wavelength is generally negligible (Huang et al., 2007). Secondly, we have assumed that the film is perfectly bonded to the substrate. The properties of the interface may influence the wrinkling behavior of the film, as discussed by Pan et al. (2009). Therefore, the theoretical results derived here may be invalid if delamination occurs.

6. Conclusions

In summary, we have investigated the surface wrinkling of a film resting on a soft elastic graded substrate engendered by in-plane compression. For the two typical situations in which the variations in the Young's modulus on the substrate are described by a power function and an exponential function, both theoretical analysis and finite element computations have been performed. Our analysis correlates the critical condition and pattern characteristics of surface wrinkling with the geometric and mechanical parameters of the system. The results may not only find applications in thin-film metrology and surface patterning but also provide insight into the formation and evolution of the surface morphology in various living tissues.

Acknowledgements

Supports from the National Natural Science Foundation of China (Grant Nos. 10972112 and 10972121), Tsinghua University (Grant No. 2012Z02103) and 973 Program (Grant Nos. 2010CB631005 and 2012CB934101) are acknowledged. The authors thank the two anonymous referees for their helpful comments and suggestions, which greatly help improve the paper.

References

ABAQUS analysis user's manual, Version 6.8, 2008.
Allen, H.G., 1969. Analysis and Design of Structural Sandwich Panels. Pergamon, New York.
Audoly, B., Boudaoud, A., 2008a. Buckling of a stiff film bound to a compliant substrate—Part I: Formulation, linear stability of cylindrical patterns, secondary bifurcations. J. Mech. Phys. Solids 56, 2401–2421.
Audoly, B., Boudaoud, A., 2008b. Buckling of a stiff film bound to a compliant substrate—Part II: A global scenario for the formation of herringbone pattern. J. Mech. Phys. Solids 56, 2422–2443.

Audoly, B., Boudaoud, A., 2008c. Buckling of a stiff film bound to a compliant substrate—Part III: Herringbone solutions at large buckling parameter. J. Mech. Phys. Solids 56, 2444–2458.
Ben Amar, M., Goriely, A., 2005. Growth and instability in elastic tissues. J. Mech. Phys. Solids 53, 2284–2319.
Bowden, N., Brittain, S., Evans, A.G., Hutchinson, J.W., Whitesides, G.M., 1998. Spontaneous formation of ordered structures in thin films of metals supported on an elastomeric polymer. Nature 393, 146–149.
Bowden, N., Huck, W.T.S., Paul, K.E., Whitesides, G.M., 1999. The controlled formation of ordered, sinusoidal structures by plasma oxidation of an elastomeric polymer. Appl. Phys. Lett. 75, 2557–2559.
Brau, F., Vandeparre, H., Sabbah, A., Poulard, C., Boudaoud, A., Damman, P., 2011. Multiple-length-scale elastic instability mimics parametric resonance of nonlinear oscillators. Nat. Phys. 7, 56–60.
Cai, S., Breid, D., Crosby, A.J., Suo, Z., Hutchinson, J.W., 2011. Periodic patterns and energy states of buckled films on compliant substrates. J. Mech. Phys. Solids. 59, 1094–1114.
Cerda, E., Mahadevan, L., 2003. Geometry and physics of wrinkling. Phys. Rev. Lett. 90, 074302-1–074302-4.
Chan, E.P., Smith, E.J., Hayward, R.C., Crosby, A.J., 2008. Surface wrinkles for smart adhesion. Adv. Mater. 20, 711–716.
Chen, S.H., Peng, C.Y., Zhang, P., Gao, H.J., 2009. Mechanics of adhesive contact on a power-law graded elastic half-space. J. Mech. Phys. Solids 57, 1437–1448.
Efimenko, K., Rackaitis, M., Manias, E., Vaziri, A., Mahadevan, L., Genzer, J., 2005. Nested self-similar wrinkling patterns in skins. Nat. Mater. 4, 293–297.
Feng, X.Q., Gao, X.F., Wu, Z.N., Jiang, L., Zheng, Q.S., 2007. Superior water repellency of water strider legs with hierarchical structures: experiments and analysis. Langmuir 23, 4892–4896.
Giannakopoulos, A.E., Pallot, P., 2000. Two-dimensional contact analysis of elastic graded materials. J. Mech. Phys. Solids 48, 1597–1631.
Giannakopoulos, A.E., Suresh, S., 1997. Indentation of solids with gradients in elastic properties: Part I. Point force. Int. J. Solids Struct. 34, 2357–2392.
Gibson, R.E., 1967. Some results concerning displacements and stresses in a non-homogeneous elastic half-space. Geotechnique 17, 58–67.
Groenewold, J., 2001. Wrinkling of plates coupled with soft elastic media. Physica A 298, 32–45.
Hendricks, T.R., Lee, I., 2007. Wrinkling-free nanomechanical film: control and prevention of polymer film buckling. Nano Lett. 7, 372–379.
Howarter, J.A., Stafford, C.M., 2010. Instability as a measurement tool for soft materials. Soft Mat. 6, 5661–5666.
Huang, R., 2005. Kinetic wrinkling of an elastic film on a viscoelastic substrate. J. Mech. Phys. Solids 53, 63–89.
Huang, R., Stafford, C.M., Vogt, B.D., 2007. Effect of surface properties on wrinkling of ultrathin films. J. Aerospace Eng. 20, 38–44.
Huang, Z.Y., Hong, W., Suo, Z., 2005. Nonlinear analyses of wrinkles in a film bonded to a compliant substrate. J. Mech. Phys. Solids 53, 2101–2118.
Jia, F., Cao, Y.P., Liu, T.S., Jiang, Y., Feng, X.Q., Yu S.W., in press. Wrinkling of a bilayer resting on a compliant substrate. Philos. Mag.
Khang, D.Y., Jiang, H.Q., Huang, Y., Rogers, J.A., 2006. A stretchable form of single-crystal silicon for high-performance electronics on rubber substrates. Science 311, 208–212.
Koch, K., Bhushan, B., Jung, Y.C., Barthlott, W., 2009. Fabrication of artificial Lotus leaves and significance of hierarchical structure for superhydrophobicity and low adhesion. Soft Mat. 5, 1386–1393.
Lacour, S.P., Jones, J., Wagner, S., Li, T., Suo, Z., 2005. Stretchable interconnects for elastic electronic surfaces. Proc. IEEE 93, 1459–1467.
Lee, D.H., Triantafyllidis, N., Barber, J.R., Thouless, M.D., 2008. Surface instability of an elastic half space with material properties varying with depth. J. Mech. Phys. Solids 56, 858–868.
Li, B., Cao, Y.P., Feng, X.Q., Gao, H.J., 2011a. Surface wrinkling of mucosa induced by volumetric growth: theory, simulation and experiment. J. Mech. Phys. Solids 59, 758–774.
Li, B., Jia, F., Cao, Y.P., Feng, X.Q., Gao, H.J., 2011b. Surface wrinkling patterns on a core–shell soft sphere. Phys. Rev. Lett. 106, 234–301.
Li, B., Cao, Y.P., Feng, X.Q., Gao, H.J., in press. Mechanics of morphological instabilities and surface wrinkling in soft materials: a review. Soft Mat.
Mei, H.X., Landis, C.M., Huang, R., 2011. Concomitant wrinkling and buckle-delamination of elastic thin films on compliant substrates. Mech. Mater. 43, 627–642.
Mueller, M.M., Ben Amar, M., Guven, J., 2008. Conical defects in growing sheets. Phys. Rev. Lett. 101, 156104-1–156104-4.
Muravskii, G.B., 2008. Response of an elastic half-space with power-law nonhomogeneity to static loads. Arch. Appl. Mech. 78, 965–987.
Pan, X.H., Huang, S.Q., Yu, S.W., Feng, X.Q., 2009. Interfacial slippage effect on the surface instability of a thin elastic film under van der Waals force. J. Phys. D: Appl. Phys. 42, 055302-1–055302-8.
Plevako, V.P., 1971. On the theory of elasticity of inhomogeneous media. J. Appl. Math. Mech. 35, 853–860.
Schweikart, A., Fery, A., 2009. Controlled wrinkling as a novel method for the fabrication of patterned surfaces. Microchim. Acta 165, 249–263.
Stafford, C.M., Harrison, C., Beers, K.L., Karim, A., Amis, E.J., Vanlandingham, M.R., Kim, H.-C., Volksen, W., Miller, R.D., Simonyi, E.E., 2004. A buckling-based metrology for measuring the elastic moduli of polymeric thin films. Nat. Mater. 3, 545–550.
Volynskii, A.L., Bazhenov, S., Lebedeva, O.V., Bakeev, N.F., 2000. Mechanical buckling instability of thin coating deposited on soft polymer substrates. J. Mater. Sci. 35, 547–554.
Wu-Bavouzet, F., Cayer-Barrioz, J., Le Bot, A., Brochard-Wyart, F., Buguin, A., 2010. Effect of surface pattern on the adhesive friction of elastomers. Phys. Rev. E 82, 031806-1–031806-9.